

# Microstructure of friction surface developed on carbon fibre reinforced carbon–silicon carbide ( $C_f/C$ –SiC)

Yuan Wang, Houzheng Wu\*

*Department of Materials, Loughborough University, Leicestershire LE11 3TU, UK*

Received 22 February 2012; received in revised form 21 March 2012; accepted 26 March 2012

Available online 18 April 2012

## Abstract

We have used TEM to study the microstructure of friction surface of carbon fibre/carbon–silicon carbide composites brake discs after multi braking stop by using organic pads. A friction surface layer was developed consistently on the top of Si regions of the composites, but inconsistently on that of SiC and C. Inside the layer, amorphous silicon/silicon oxides appeared extensively with various non-metallic and metallic crystallites dispersed inside with sizes ranging from a few nanometers to several microns. A coherent interface between the friction layer and the composite surface was established under the braking conditions, whilst its sustainability varied notably in SiC and C regions. Microcracking near the friction surface appeared in SiC and  $C_f/C$  regions largely due to the extensive ductile deformation of SiC and weak interfaces between C and  $C_f$ . Material joining mechanisms were discussed to enlighten the friction transfer layer development on the surface of the composite discs.

© 2012 Elsevier Ltd. Open access under [CC BY license](http://creativecommons.org/licenses/by/3.0/).

**Keywords:** Composites; Electron microscopy; Surfaces; SiC; Carbon fibre

## 1. Introduction

Carbon fibre reinforced carbon–silicon carbide ( $C_f/C$ –SiC) composites have been continuously developed as friction materials for brakes of road transport vehicles since their initial commercial success over a decade ago.<sup>1</sup> However, existing knowledge is often unable to offer enough scientific rationale on the friction performance for a brake that includes a given carbon fibre ceramic as the disc and a chosen friction material as the pads. This situation could hinder the attempts to optimise the potential of ceramic composites as brake discs, as well as to develop suitable pads for such discs. For a while, much of the research attention has been given on the impact of carbon fibre architecture or microstructure of the composites on their mechanical and physical properties. For instance, several publications focused on the impact of carbon fibre architecture and ceramic constituents on the strength, toughness, thermal conductivity and specific heat capacity of the composites. Whilst these material properties do have certain influence on the friction performance and wear resistance of

the composites, the interactions between the composite and the friction materials of pads largely dictate the ultimate friction performance of the brakes. Up to now, however, only limited study has been available in literature on the friction surface of ceramic matrix composites (CMCs) brake discs, including carbon fibre reinforced ceramic composites.<sup>2,3</sup>

Recently, we presented a fairly systematic observation of the development of friction surface on carbon fibre ceramic composite discs, when a pad made of organic friction material was used to stop the rotating discs.<sup>4</sup> It was noticed that, from very early on, friction surface was subjected to significant development during braking. Whilst the transferred materials, mainly contributed from the pad, deposited on the surface of the discs, their existing format and sustainability demonstrated a strong dependence on the constituents in the composite and surface structure of the discs. It was likewise noticed that fracture occurred extensively on the friction surface, which might have had a significant impact on the deposition of transferred materials, and the premature failure of friction transfer layer, if any. Though friction transfer layer has not generally been emphasised in understanding the friction performance of carbon fibre ceramic discs, some studies did notice the appearance of transfer layers.<sup>5</sup> Fracture on the friction surface, particularly in carbon fibre/carbon ( $C_f/C$ ) regions, had also had the attention of researchers.<sup>6</sup> However, detailed

\* Corresponding author. Tel.: +44 1509 223342; fax: +44 1509 223949.  
E-mail address: [h.wu2@lboro.ac.uk](mailto:h.wu2@lboro.ac.uk) (H. Wu).

understanding is yet unavailable of the observed deposition of transferred materials.

In traditional brakes including grey cast iron as the discs and organic friction materials as the pads, friction transfer layers are developed on the friction surfaces, and it is these transfer layers that dictate the friction performance of the brakes.<sup>7</sup> Knowledge on these friction transfer layers has been accumulated for more than three decades already.<sup>8</sup> It is recognised that the stability of the friction layer on the sliding surfaces depends on the cohesive bond strength of the friction layer itself, as well as that between the layer and the surface of disc. It is also generally agreed that stable friction surface is needed for stable friction, low wear rate, noise- and vibration-free performance across a wide temperature regime,<sup>7,8</sup> which directly influence the users' safety, comfort and durability. With the progress of characterisation techniques such as focused ion beam microscopy (FIB) and transmission electron microscopy (TEM), the microstructure of the transfer layers, and therefore the cohesive bond inside the friction film, have been studied with more details most recently. These studies indicated that the transfer layers were composed of nanocrystalline microstructure developed through strong interactions among mechanical mixing, oxidation and severe deformation of the matters on the friction interface.<sup>9–12</sup> It was also demonstrated that the existence of friction transfer layer was a consequence of dynamic equilibrium between initiation, growth and degradation of contact patches.<sup>11,13</sup> There is little knowledge on the bonding between the friction transfer layer and the discs and pads, whilst a discernable friction transfer layer and a fragmented layer were recently discerned on the surface of grey cast iron.<sup>14</sup> This situation might be due to a belief that bonding should not be a problem in traditional brakes, whilst it could become problematic for CMC brake discs.

In this study, we will expose the details of the friction surface of the ceramic composites by analysing the cross section with TEM. The results of the examination may imply if a robust and strong friction layer can be developed on the surface of carbon fibre ceramic composites brake discs, which might shed light on the observed difference in friction performance among brakes. The study may also benefit any attempts to re-design CMCs for friction application.

## 2. Experimental procedures

### 2.1. Materials and friction surfaces after testing

The C<sub>f</sub>/C–SiC used in this study was supplied by Surface Transforms (UK). The composites were manufactured through chemical vapour infiltration (CVI) to generate carbon fibre/carbon (C<sub>f</sub>/C) preforms first, where almost all spaces inside carbon fibre bundles were fully filled in with pyrolytic carbon, and all bundles were wrapped with a layer of pyrolytic carbon. Such preforms were then infiltrated with silicon melt at a temperature above its melting point in an inert atmosphere, normally argon.

The as-received C<sub>f</sub>/C–SiC composite blocks were cut into discs in laboratory with a diameter of 50 mm and a thickness

of 10 mm. All testing surfaces of the discs were finished by polishing with 3 μm diamond paste after multi step grinding by applying a series of diamond grits with a size of 68, 26 to 15 μm to remove a thickness of about 300–400 μm per step, which should be more than enough to eliminate any mechanical damages left from grinding steps.

The friction material for brake pads was selected from products of Federal-Mogul Friction Products Ltd. (UK). This material should belong to the organic type, as so called in industry, and its essential characteristics will be highlighted in Section 3.2. The material was mounted on a steel back plate in a ring shape with an outside diameter of 48 mm, inner diameter 40 mm, and thickness 12 mm. The surfaces of the pads were finished by grinding with a grinding wheel consisting of SiC abrasives with a grit size of 3 mm.

The friction tests were conducted on a laboratory scale dynamometer. Under an established testing regime, the key parameters were set as followings: braking pressure was 0.9 MPa, rotating speed of the disc before braking ~25 m/s at the outside boundary of the friction track. Such a set-up on a small scale dynamometer was inside the test regime for most vehicle-based tests, apart from the size of the braking area was significantly scaled down. The coefficient of friction (CoF) for each discrete braking stop was the averaged value of all acquired data with a data logging frequency of 50 Hz from the first touch by the pad to complete stop of the disc. Accumulated braking stops of 49 were accomplished for each braking couple, and the friction surface of the discs after the last stop was the interest of this paper.

### 2.2. Surface characterisation of the friction surface

#### 2.2.1. Top surface

Optical microscopy (OM) (MeF3, Reichert-Jung, Wien, Austria) was used to image the virgin surface after polishing and the friction one after dynamometer testing. The key phases, e.g. silicon carbide, graphite, silicon and carbon fibre filaments were differentiated by the contrast under polarised lighting and differential interference contrast (DIC) conditions. SEM/EDX analysis of friction surfaces were accomplished on a field emission scanning electron microscope (Leo S360, Cambridge Instruments, Cambridge, UK). In most cases, the operating electron acceleration voltage was set to 5 kV; other voltages could be chosen whenever further information was needed.

#### 2.2.2. Cross section of surface

Cross section TEM samples were made on the friction surface with FIB (FEI, FEI Nava 600 nanolab, OR, USA) using the following procedure:

- (a) First, a 1 μm thick platinum coating was deposited on the interested region of the friction surface, so as to prevent Ga<sup>+</sup> implantation and sputter erosion of the top portion of the surface.
- (b) A rectangle trench was dug adjacent to the platinum strip using a 20 nA 30 kV Ga<sup>+</sup> ion beam.

- (c) When the trench was large enough, the second trench adjacent to the other side of the platinum strip was dug under the same condition. Before the thickness of the wall reduced to about  $2\ \mu\text{m}$ , both sides were milled using a  $7\ \text{nA}$   $30\ \text{kV}$   $\text{Ga}^+$  beam to clean and smooth the surfaces of the cross section.
- (d) The membrane for TEM was then lift out and welded on Cu or Mo grits after cutting off from the bulk using the ion beam.
- (e) A final thinning process was carried out using a  $1\ \text{nA}$   $5\ \text{kV}$   $\text{Ga}^+$  beam at an inclined angle of  $1.5^\circ$  to the surface of the membrane, to minimise the depth of any residual damage by the ion beam, if any.

The typical thickness made by following this procedure was about  $200\ \text{nm}$ .

TEM observation and chemical element identification were carried using a JEOL 2000F (JEOL, Japan) with EDX probe (Oxford Instrument, UK), under a high tension of  $200\ \text{kV}$ .

### 3. Experimental results

#### 3.1. Friction performance

The measured coefficient of friction (CoF), averaged from recorded data of four pairs of disc and pad, is available from our previous paper<sup>4</sup> for every single braking applied from the 1st to 49th. The highest CoF of  $0.33 \pm 0.01$  was achieved at the last braking stop, which was raised from a starting level of  $0.27 \pm 0.01$  at the first one. Whilst the friction had not yet reached to a sustainable stage of friction under the current test regime, the amount of increment of the measured CoF slowed down significantly after 25 braking stops. We believe that the bedding, a process for building up a stable friction, had made a significant progress after 49 braking stops under the current test conditions.

#### 3.2. Overview of pad lining materials

Exemplary microstructure of friction material chosen for brake pad of this study is shown in Fig. 1. The following chemical elements were detected using SEM/EDX: Fe, Cu, Zn, O, Si, Mg, Al, S, Sn and Ca. The key constituents in the formulation included metallic materials such as copper and steel, abrasives like alumina and silicon carbide, as well as graphite and a small amount of minerals. All these constituents, including polymeric fibres were bonded together by phenolic resin. Like any other commercial organic pad materials, it is difficult to precisely define the composition as each supplier has its own specific formulation with certain modification.

#### 3.3. Carbon fibre ceramic composites discs before and after braking testing

Optical microscopy image of the as-polished surface (Fig. 2(a)) revealed the microstructure of the bulk composite: carbon fibre bundles were approximately laid on the finished

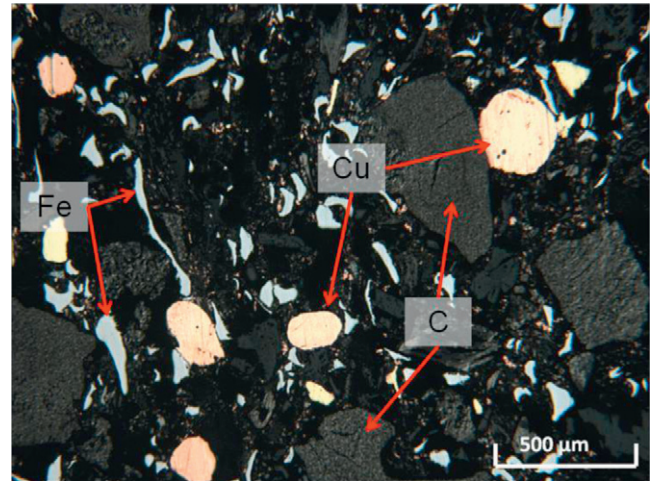


Fig. 1. An overview of the microstructure of friction material for the pads. Key chemical elements include C, Fe, Cu, Zn, O, Si, Mg, Al, S, Sn and Ca.

plane, i.e. friction surface; silicon carbide and silicon region (abbreviated as SiC + Si thereafter) existed among the fibre bundles that themselves were nearly fully wrapped by pyrolytic carbon; a small amount of carbon fibre bundles were in perpendicular direction, which needed the carbon fibre felts together before applying CVI. The averaged area fraction of SiC and Si regions was  $14.8 \pm 3.8\%$  and  $3.2 \pm 2.2\%$  respectively on the

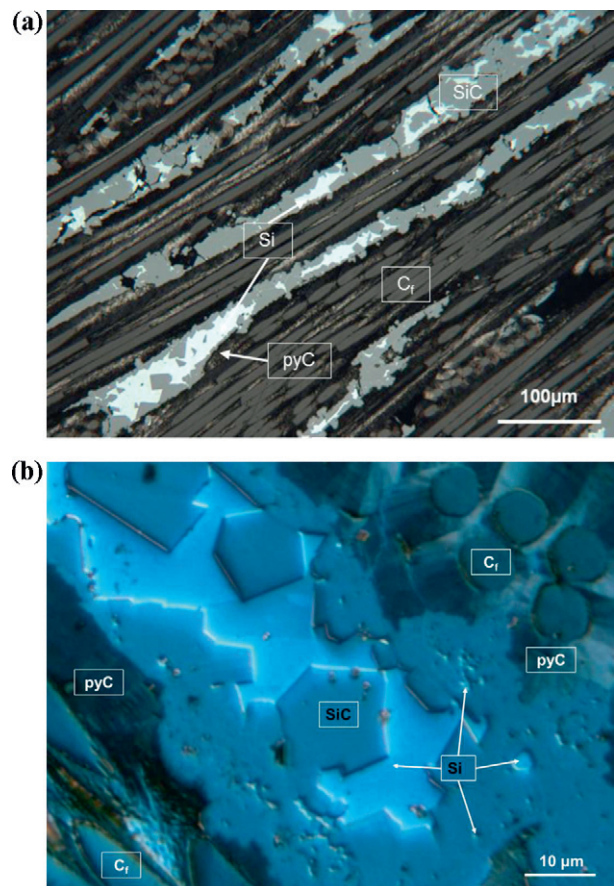


Fig. 2. Optical microscopy images of (a) as-polished surface and (b) etched surface with diluted HF solution.

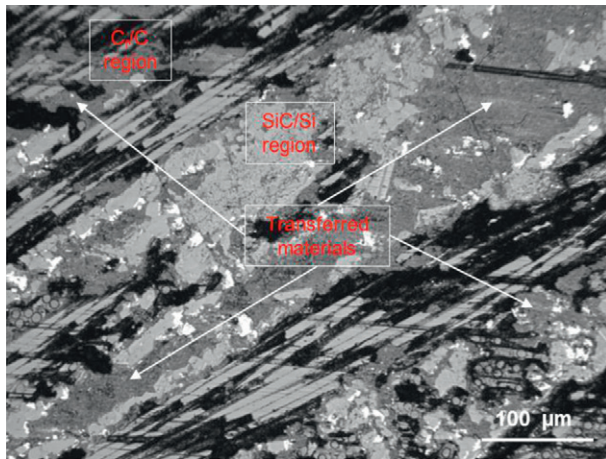


Fig. 3. Optical microscopy images of friction surface after 49 braking stops on dynamometer. Transferred materials are indicated in SiC/Si and Cf/C regions.

friction surface, whilst their distribution and sizes were fairly heterogeneous. Indeed, the shape and size of a SiC + Si region is likely defined by the nature of the open channels that exist inside the carbon fibre/carbon performs. The amount of Si and its distribution in each SiC + Si region were possibly decided by the carbonisation process and the supply of carbon, which was a topic of other studies.<sup>15</sup> It is believed that during the melt infiltration, the contact regions between Si melt and pyrolytic carbon could be converted into SiC regions fairly quickly through a carbonisation process of Si.<sup>15,16</sup> The degree of carbonisation should be controlled by the kinetics of C diffusion through SiC product and the supply of the two chemicals; it is therefore not unusual to see significant amount of residual Si and pyrolytic C existing in the microstructure of the composites. It was noticed that voids and cracks appeared on the surface, which was likely introduced by the surface finish operation, if not all left by manufacture process. Under high magnification, as shown in Fig. 2(b), some small pockets of silicon scattered among SiC crystallites, apart from the large Si “lakes” surrounded by SiC. The contrast in pyrolytic carbon wrapping around the vertical carbon fibres was formed by the polarised lighting condition, indicating the degree of graphitisation of the carbon.<sup>17</sup>

After up to 49 braking stops on the dynamometer, transferred materials were mostly deposited in SiC + Si regions, as shown in Fig. 3. Detailed observation on the depositing process has been published in an early paper through a series of focused examinations on the friction surface after applying a certain number of braking stops.<sup>4</sup>

#### 3.4. Cross section on the friction surface of carbon fibre/carbon regions

Previous SEM/EDX analysis of the friction surface of Cf/C regions had demonstrated that most transferred materials existed in a crumbled format inside topographically lower places, whilst some carbon fibre surfaces showed clear abrasive wear tracks only.<sup>4</sup> It was also noticed that transferred materials could fill in around interfaces between carbon fibres and carbon matrix, particularly in regions containing vertical fibre filaments. Cross

section in this region was examined using TEM, and typical features are summarised in Fig. 4(a) with an inset of SEM image showing the surface morphology in a top view.

TEM examination confirmed that no continuous layer or film of any transferred materials bonded on the surface of either pyrolytic carbon or carbon fibres. Only a thin layer of amorphous carbon with an estimated thickness of  $\sim 50$  nm appeared on the top friction surface of carbon fibres, as shown in Fig. 4(b). This layer should be the similar one as that observed on the friction surface of carbon fibre reinforced carbon composites (CCC).<sup>18,19</sup> It was noticed that a small amount of debris occasionally penetrated into the surface of the carbon fibre, but with a depth inside  $\sim 200$  nm, as shown in Fig. 4(b).

On the Cf/C interfaces where transferred materials existed like fillers (inset in Fig. 4(a)), the TEM images revealed that these transferred materials did penetrate into a position with a depth of  $\sim 2$   $\mu\text{m}$ , as shown in Fig. 4(a). A scale of the transferred materials, with a thickness of  $\sim 0.1$   $\mu\text{m}$  remained on the top of friction surface, as shown in Fig. 4(c), and the main chemical elements included Fe, Cu, Al, Si, S, C and O, which are the major elements detected in the friction material of pad. Along the two Cf/C interfaces, there existed a string of fine silicon carbide particles (approved by EDX), with a size range from tens to hundreds nanometers. These silicon carbide particles were mostly separated by the similar transferred materials as shown on top layer. Stuck between the two strings of transferred materials, a carbon region, with a width of about  $0.4$   $\mu\text{m}$ , was actually part of the pyrolytic carbon matrix, because the selected area diffraction patterns from there give same lattice distance between (0003) crystal planes and same broadening level of (0003) diffraction spot as in pyrolytic carbon matrix.

Underneath the Cf/C region, micro-cracks were initiated along the interface between fibre and matrix, whilst no crack was noticed inside either fibre or matrix.

#### 3.5. Cross section on friction surface of silicon regions

##### 3.5.1. Interface between transfer layer and silicon substrate

The cross section structure of friction surface developed in a Si region is shown in Fig. 5(a). A layer of transferred materials was clearly bonded by an interface region along the surface of Si. Some discrete gaps appeared at the arrowed positions in Fig. 5(a); EDX analysis confirmed that the detached materials from surface of silicon region were iron, such as particle P2. For the bonded regions on the interface, EDX results clearly indicated that copper particles were linked with surface of silicon, e.g. P1 in Fig. 5(a). To have further details across the bonded interface, the chemical compositions were detected across the interface at positions A, B and C, as shown in Fig. 5(b). Visually, position B was more close to the interface between the transferred materials and Si. The detected chemical compositions at the three positions are plotted in Fig. 5(c). At position A, the molar ration of Cu/Si was 4.1, but no detectable oxygen; at B, the Cu/Si ratio was reduced to 1.2 and O/Si ratio approached to 1.7; at C, the Cu/Si was further reduced to 0.2 and O/Si to 0.8.

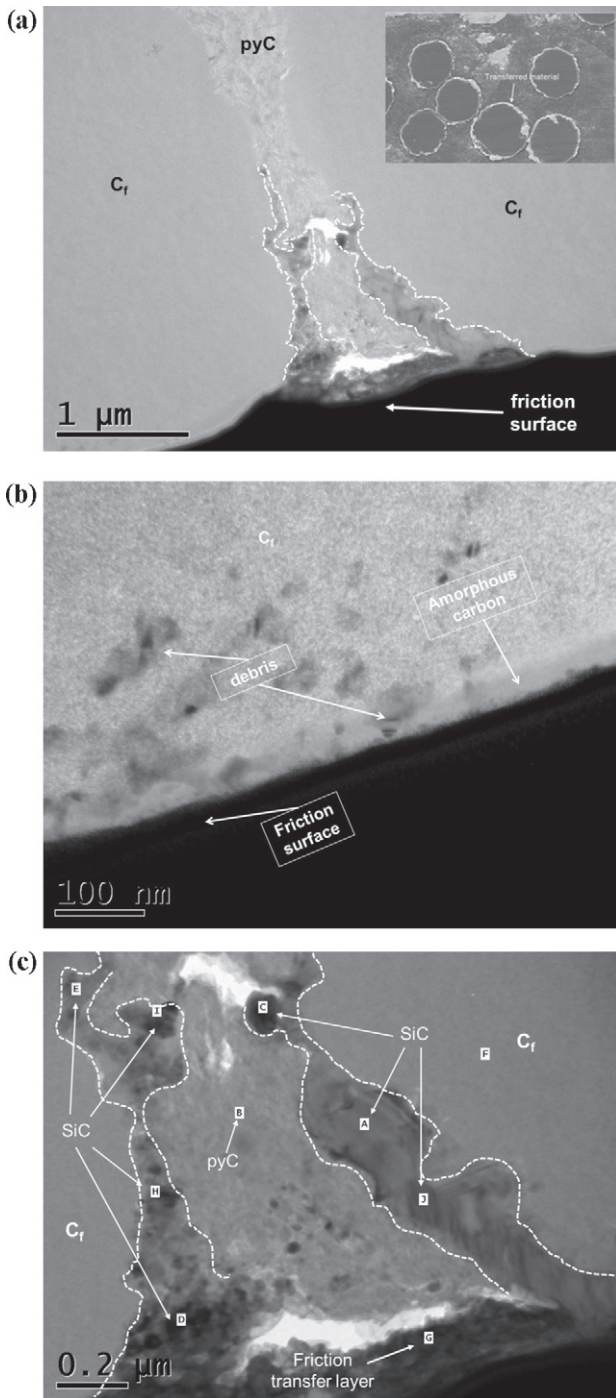


Fig. 4. (a) Cross-section TEM microstructure of friction surface in  $C_f/C$  regions where fairly dense materials had filled in between carbon fibre ( $C_f$ ) and pyrolytic carbon (pyC) matrix (SEM image of friction surface in  $C_f/C$  region is shown in the inset); (b) a layer of amorphous carbon was developed on the friction surface of carbon fibre and some ceramic debris, shown in darker contrast under diffraction contrast imaging condition, penetrated into the carbon fibre; (c) more details around the interfaces where transfer materials were deposited. The dashed lines in (a) and (c) indicate the boundaries between carbon constituent ( $C_f$  or pyC) and transferred material. The letters from A to E and H to I in (c) marked the positions where SiC constituents were confirmed by EDX, F where only carbon was confirmed, and G where key chemical elements that exist in the pad were detected.

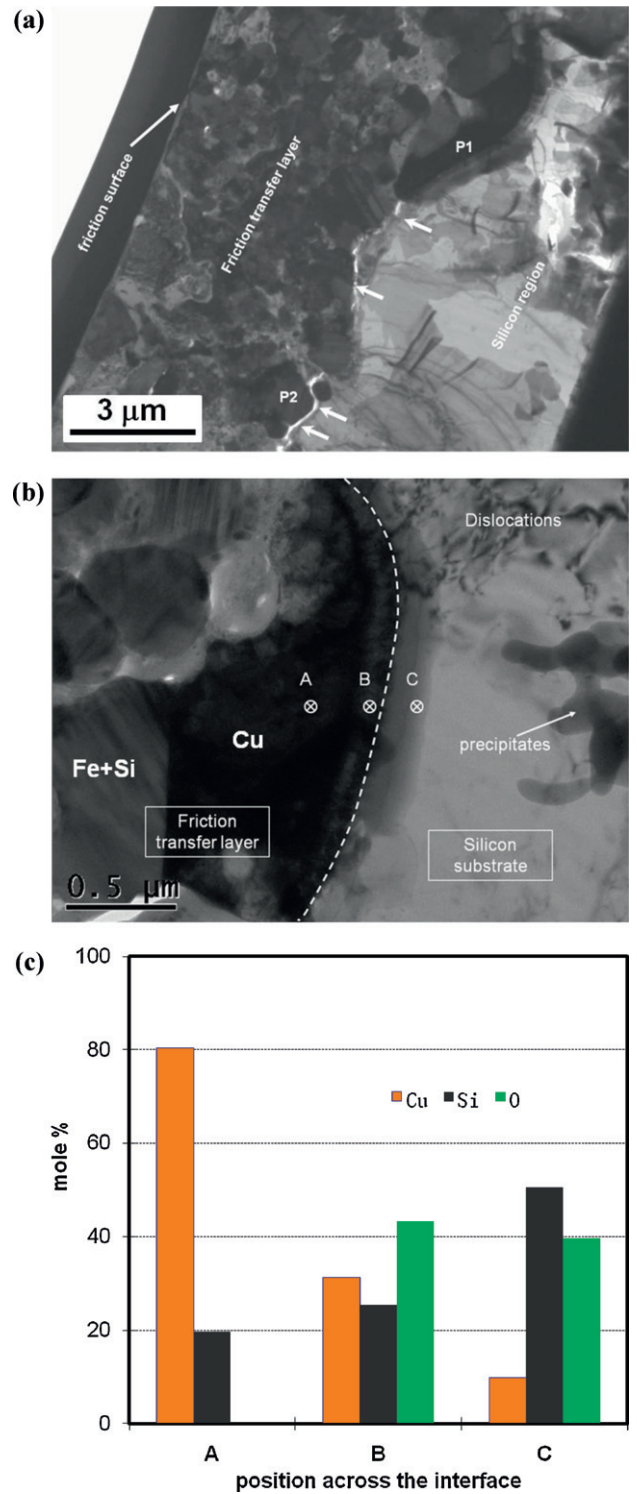


Fig. 5. Cross section TEM image on the friction surface of a silicon region. (a) A friction transfer layer was bonded on the surface of silicon. Arrows indicate gaps existing on the interface. Particle P1 that fused with silicon consists of copper, and particle P2 that detached from the silicon consisted of iron, as confirmed by EDX. (b) Characteristics in the near surface of Si include: fusion with transferred material; oxygen enriched precipitates in flake morphology; dislocations. (c) Variation of chemical elements across the fused interface, as indicated in (b).

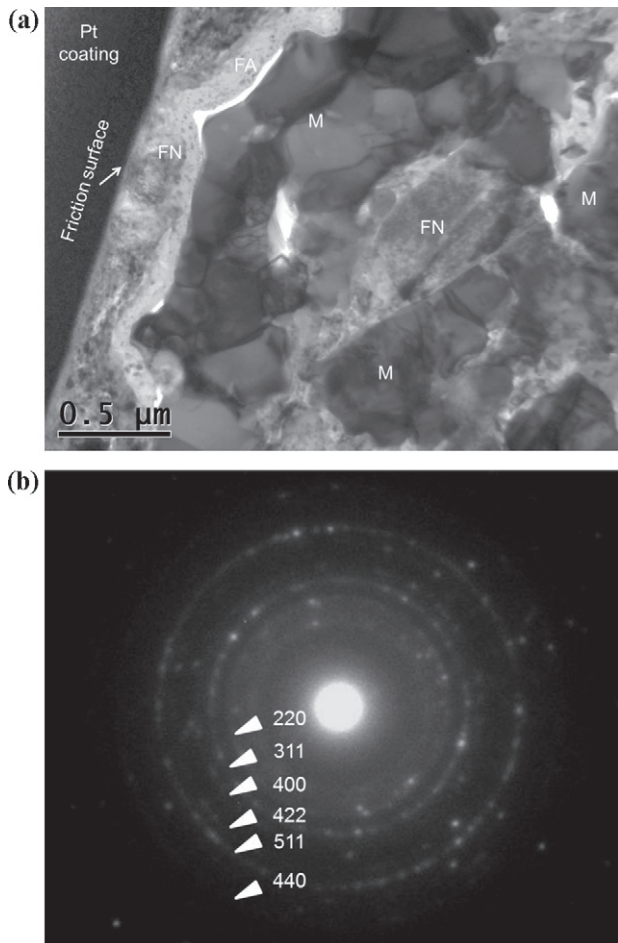


Fig. 6. Cross section microstructure of the friction transfer layer deposited over the Si region. (a) Exemplary microstructure shows the existence of metallic debris (marked as M) consisting of iron and silicon, and nano-sized crystallites zones (FN) consisting of O, Fe, Si, Cu, Zn, Mg and Al; (b) selected area diffraction pattern from nano-sized crystallites zone shows the existence of magnetite crystallites, with indices of magnetite included.

Beyond position C, O/Si ration was further reduced; most of the region has no detectable oxygen.

### 3.5.2. Transfer layer

As shown in Fig. 5(a), the transfer layer was developed with a thickness of a few microns, but varied with the contour of the surface of Si substrate to keep the friction surface on the same level. An exemplary microstructure of the transfer layer near the friction surface is presented in Fig. 6(a). It was composed of metallic crystallites (called M particles or regions hereinafter), marked as M, and fine particulate zones (called F zones), marked as FN or FA, the types of F zones defined by characteristics existing in these zones.

In the M zones, most comprised iron-based alloys, but some consisted of copper/copper-based alloys; their sizes ranged from sub-micron to a few microns. EDX detected significant amount of Si in M zones that contained Fe, though the Si/Fe ratios varied from site to site. A copper zone was marked in Fig. 5(b) without Si detected, whilst the neighboured iron alloy contained substantial Si (marked as Fe + Si). Within the debris, dislocations

and sub-grain boundaries existed extensively, along with high angle grain boundaries. The sizes of the polygonised zones or refined grains were around a couple of hundreds nanometers.

In the F zones, two types can be distinguished. The first type comprised densely packed nanocrystallites (called FN zone). Two FN zones were marked in Fig. 6(a). Representative chemical elements, probed with EDX, include Fe, Zn, O as majority and Mg, S, Si and Al as minority. The crystallinity of these zones was demonstrated by the selected area diffraction pattern (SADP), as shown in Fig. 6(b). As the crystallites were very fine and mixed with different crystals, it was difficult to resolve more details; the estimated particle size might have been around tens nanometers. By indexing SADP and considering the detected chemical elements, we can deduce that this FN zones were mainly composed of magnetite ( $\text{Fe}_3\text{O}_4$ ) nano-crystallites, including a small amount of other mineral ones, mainly used as lubricants/fillers in the pad liner. Note, the 1 1 1-ring of magnetite became invisible in Fig. 6(b) due to a bright central spot, but it did appear in other diffraction patterns that we took from similar regions.

The second type of F zones existed widely inside the transfer layer, called FA zones where amorphous silicon appeared with nano-sized crystallites dispersed. The FA zones were more transparent than FN ones under the same electron lighting condition. An example is shown in Fig. 7. EDX analysis showed that inside the circled area A, key chemical elements included Si, O and Fe, and in area B, only Si and O; the O/Si ration was variable, but less than 1. SADPs from both area A and B are shown in Fig. 7(b) and (c). From all these experimental evidences, we can infer that the nano-dispersants in these FA zone were  $\text{Fe}_3\text{O}_4$  crystallites, and the matrix was amorphous Si, where oxygen could exist in various quantities. Most of these FA zones were found in a region among metallic particles, as seen in Fig. 7(a). It was also noticed that FA zone existed between the FN and M zones, e.g. the relatively narrow band interfaced between FN and M zones, as shown in Fig. 6(a). With even high magnification, the FA zones were seen in much smaller scale among the M zones, as well as between F and M zones. It is clearly demonstrated that amorphous Si liked a bonding agent widely existing inside the transfer layer. Direct bonding between metallic particles was also noticed. An example is shown in Fig. 5(b) where the iron alloy particle was directly bonded with a copper particle.

### 3.6. Cross section on friction surface of silicon carbide regions

Exemplary cross section microstructure of the friction surface in SiC regions is shown in Fig. 8(a). The transfer layer and the SiC were differentiated with EDX information and/or crystal defects in SiC that could be highlighted under chosen diffraction contrast imaging condition. In Fig. 8(a), there were three regions embedded with a transfer layer, marked as TL; others were SiC only on the friction surface, marked as SiC. Clearly the transfer layers were patched, deposited in craters on the surface, with a thickness up to  $\sim 2 \mu\text{m}$ . Therefore, it was very likely that the

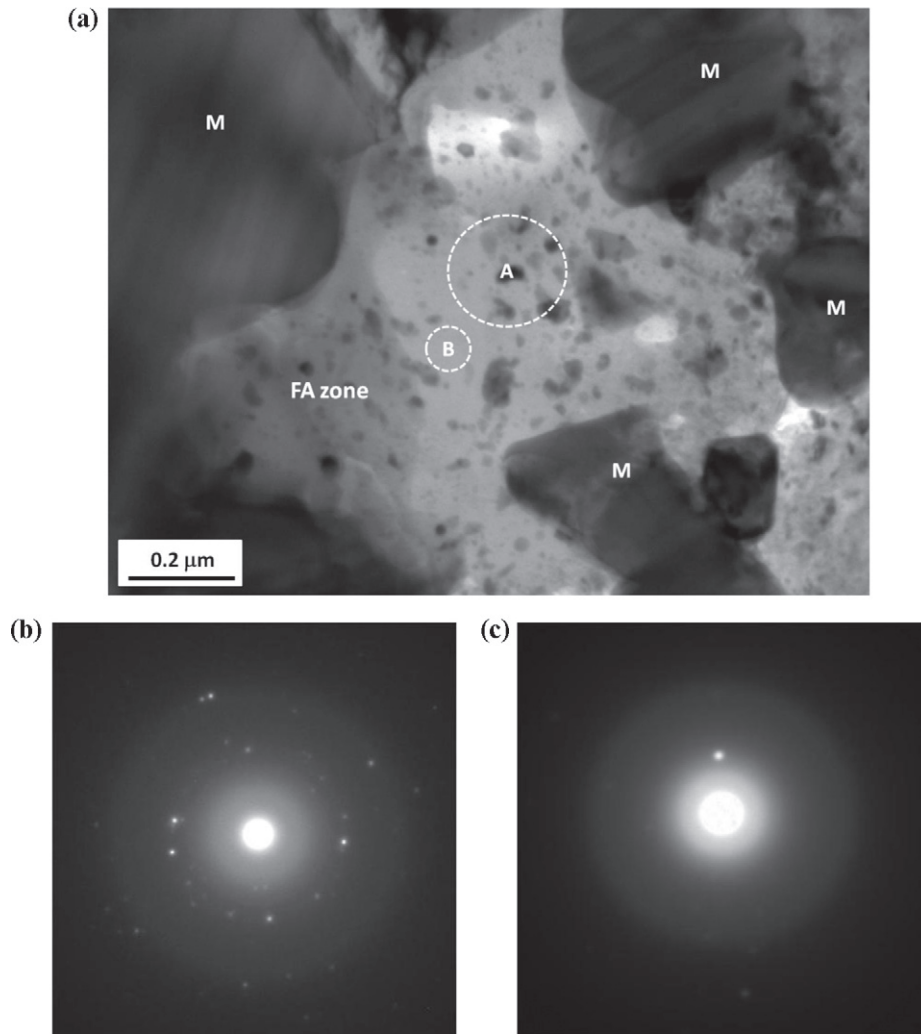


Fig. 7. Typical FA zone inside the transfer layer where nano-sized crystallites disperse inside amorphous silicon. (a) TEM image showing the FA zone sitting among metallic particles; (b) and (c) selected area diffraction patterns from regions A with crystallites included, and B without crystallites.

shape and size of the patches of the transferred materials were defined by the craters themselves.

More details on the transfer layer in SiC region is presented in Fig. 8(b). The transfer layer, separated by a dashed white line from SiC region, rooted inside a crater. The layer was composed of three M particles and one F region. EDX examination indicated that the key chemical elements of the M particles were Fe and Si. A range of chemical elements were detected in the F region, including O, Mg, Al, Si, P, S, Sb, Ca, and Fe. The integrity of the interface between the debris and the SiC crystallites were reasonably maintained, which may imply a strong bonding.

The SiC particles around the transferred materials, as well as others on the friction surface were heavily deformed with all of them bearing significant amount of slip bands/stacking faults, as shown in Fig. 8(a) and (b). It seems that underneath the surface, the SiC crystallites had experienced a severe mechanical deformation, as indicated by the amount of crystal defects and strain contours under the diffraction contrast imaging condition. Domains with sub-grain boundaries were developed in SiC grains; their size was around sub-microns to microns, as shown

in Fig. 8(a) and (b). A large crack was seen that went through the region underneath the surface by following a transgranular fracture path, as arrowed in Fig. 8(a).

#### 4. Discussion

Experimental evidences have demonstrated that when a pad was applied on a rotating  $C_f/C$ -SiC composite disc, a continuous transfer layer was successfully developed in contacted Si regions, but only a small amount of patches in SiC and C regions. Whilst Si accounted for <10% of the total surface area for the composite studied here, it can be much higher than the current level for other commercial  $C_f/C$ -SiC composites. To understand the sustainability of any transfer layers on the surface, it is necessary to appreciate the followings under the current braking context:

- (a) the cohesion inside the friction transfer layer;
- (b) the cohesion between transfer layer and surface of brake disc.

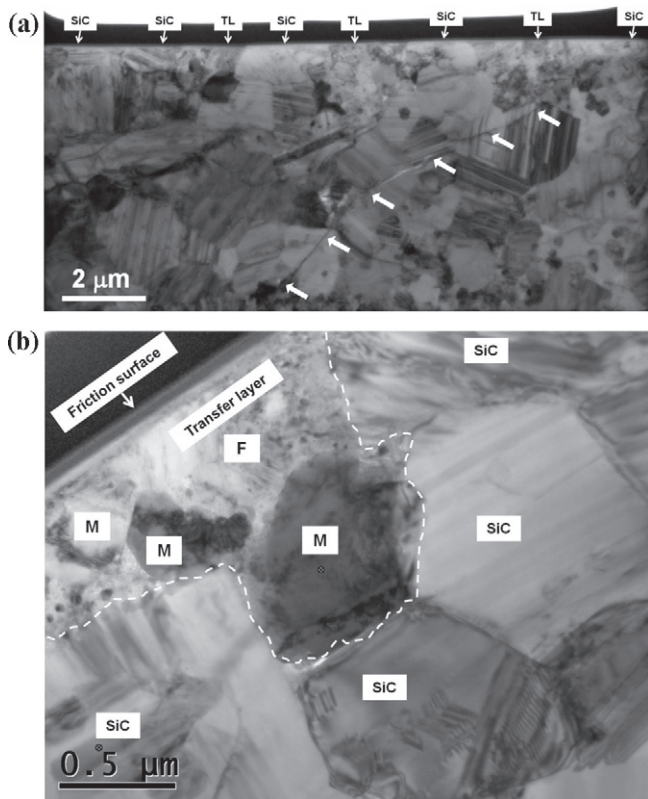


Fig. 8. Cross section TEM microstructure of friction surface in silicon carbide region. (a) An overview of the surface composed of transfer layer (TL) and silicon carbide (SiC); (b) Details on the transfer materials embedded in SiC regions where M represent the metallic debris and F the region including nano-sized crystallites. The arrows in (a) indicate the propagating path of a large crack with one end at the interface between transferred material and the SiC substrate; the dashed line in (b) outlines the boundary between transferred materials and the SiC substrate.

#### 4.1. Inferred temperature and pressure for cohesion development inside the friction transfer layer

Outcomes from TEM/EDX analysis have demonstrated that the deposited transfer layer includes metallic debris (M) and fine-grained zones (F). The schematic structure of the transfer layer is shown in Fig. 9. It is reasonably supported by the TEM observation (e.g. Fig. 6(a)) that the structure is characterised by an intercalation of the M and F zones. The cohesion of the structure should hence be established by the bonding among these distinctive zones, as well as that inside the zones under certain temperature and pressure conditions during braking, which are generally difficult to know. Here we are trying to infer these conditions from the exposed microstructure features in metallic debris in the transfer layer.

Inside the M zones, Fe and Si (Fe + Si) were widely detected together, but Fe or Cu alone, or Cu + Si was less frequently. These zones are comprised of sub-grains, as shown in Figs. 5–6, and we accordingly believe that a dynamic recovery and/or recrystallisation must have occurred in the metal debris under certain temperatures and pressures,<sup>20</sup> which should be defined by the braking operation.

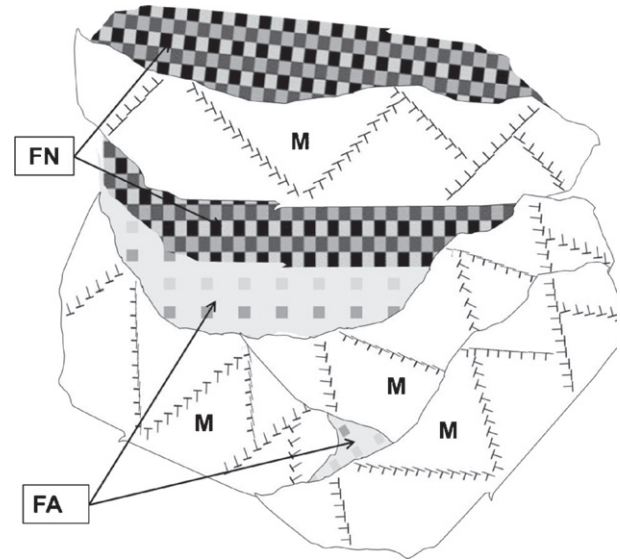


Fig. 9. Schematic of the internal structure of friction transfer layer developed on the surface of carbon fibre ceramic composite disc when organic friction material was used as pad. In the schematic, the “M” represents metallic crystallites, “FN” densely packed nano-sized crystallites, “FA” the amorphous silicon dispersed with nano-sized crystallites, “T” the dislocation, and the arrays of “T”’s indicate sub-grain boundaries or high angle grain boundaries.

As dynamic recovery/recrystallisation happens, the mean subgrain size ( $d$ ) is found to be strongly dependent on the deformation stress ( $\sigma$ ) and only weakly on temperature. It is therefore possible to estimate the applied pressure during braking by applying following relationship<sup>21</sup>:

$$\frac{\sigma d}{\mu b} = K \quad (1)$$

where  $K$  is a constant (for metals,  $K \approx 10$ ),  $\mu$  the materials shear modulus, and  $b$  the Burgers vector. By using an estimated  $d$  of  $\sim 250$  nm from Fig. 6(a), the deformation stress could be  $\sim 770$  MPa, given  $\mu$  and  $b$  a value of 77 GPa and 0.248 nm respectively for steel. The estimation implies that the transferred material can subject to a pressure 2–3 orders larger than the normal pressure applied on the brake.

It is recognised that dynamic recrystallisation should start at a temperature  $>0.8 T_m$  ( $T_m$  the melting point of a crystal)<sup>21,22</sup>.  $T_m$  for mild steel is  $\sim 1370$  °C, and the eutectoid temperature for Fe–Si binary system is  $\sim 1194$  °C at a Si/Fe ratio of  $\sim 0.5$ .<sup>22</sup> We accordingly infer that a minimum temperature of  $\sim 1000$  °C might have been achieved on the friction surface during braking.

Note that the above inference can be applied to understand the development of the cohesion inside the transfer layer, whilst the real conditions, particularly the pressure, can hardly be validated by experimentally testing.

In the FN regions, one of the two subtypes of F zones, nanocrystal  $\text{Fe}_3\text{O}_4$  and other minerals from the pad are likely developed through a tribochemical process. Under the inferred temperature and exceedingly high pressure during braking, it is not unreasonable to assume that these nano-sized particles can be packed together through a sintering process. In the FA regions, another subtype of F zones, the cohesion is clearly

defined by the amorphous Si itself, as shown in Figs. 6 and 7. We have yet no evidence to show how these FA regions were developed, but it is well-known that amorphisation in Si can be realised even at ambient temperature when extremely high pressure, e.g. this underneath sharp indenter, is applied.<sup>23</sup> It is reasonable to assume the required pressure for the amorphisation of Si would decrease as the temperature rises from room temperature. Therefore, the inferred high pressure and temperature inside the transfer layer might have been high enough to have the amorphous Si developed. At the same time, this amorphous Si could provide enough flowing capability to allow those fine crystallites dispersed inside to form the typical FA regions, as observed in Figs. 5 and 6.

The cohesion between the zone is likely developed through a welding process under the inferred high temperature and pressure, a mechanism that is widely believed by researchers who studied the structure of friction transfer layers on the surface of cast iron discs or organic pads.<sup>14</sup> We also anticipate that the existence of silic constituents, such as Fe + Si, Cu + Si, can be beneficial to bond metallic debris as Si can normally reduce the surface tension.<sup>24</sup> However, more experimental details are needed in order to understand the roles of Si on the development of the transfer layer from this perspective. It is worth noting that the detected Si was likely from the composites, as no silicon, apart from SiC, was found in the pad formulation.

#### 4.2. The cohesion between transfer layer and the constituents in the disc

Two possible joining mechanisms can be borrowed from material joining sector to understand possible bondings between transfer layer and the surface of disc: *fusion and brazing joining*.

Fusion joining involves melts of materials. On the disc surface, SiC and C have no melting but subliming when temperature is high enough. However, when oxygen is involved, SiC can be oxidised into SiO or SiO<sub>2</sub>; these oxides may fuse with other oxides or compounds that exist in the transferred materials or oxidising variants of some constituents, such as FeO<sub>x</sub>, CuO<sub>x</sub>, Al<sub>2</sub>O<sub>3</sub>, MgO, as long as the temperature is high enough. Fusion between silicon oxides and other oxides has been claimed to generate silicates by previous tribological studies.<sup>25</sup> However, it is noted that melt cannot appear in a ternary system like FeO–Fe<sub>2</sub>O<sub>3</sub>–SiO<sub>2</sub> until the temperature approaches to just under 1300 °C, as shown in Fig. 10(a). We have no evidence to support that such a level of temperature achieved on the friction surface, nor experimental details to demonstrate such silicates existing on the interface between SiC and the transfer layer.

However, melt could appear under 1100 °C for a Cu–O–SiO<sub>2</sub> ternary system, as isotherm cross section phase diagram shows in Fig. 10(b).<sup>26</sup> These facts indicate that if any fusion occurs on SiC surface via its oxidised variant, a temperature of more than 1000 °C is necessary. Therefore, when a friction material contains both steel and copper, cuprous/cupric melts can be formed at relatively lower temperatures than ferrous ones, if any transfer layer is bonded on the surface of SiC through fusion.

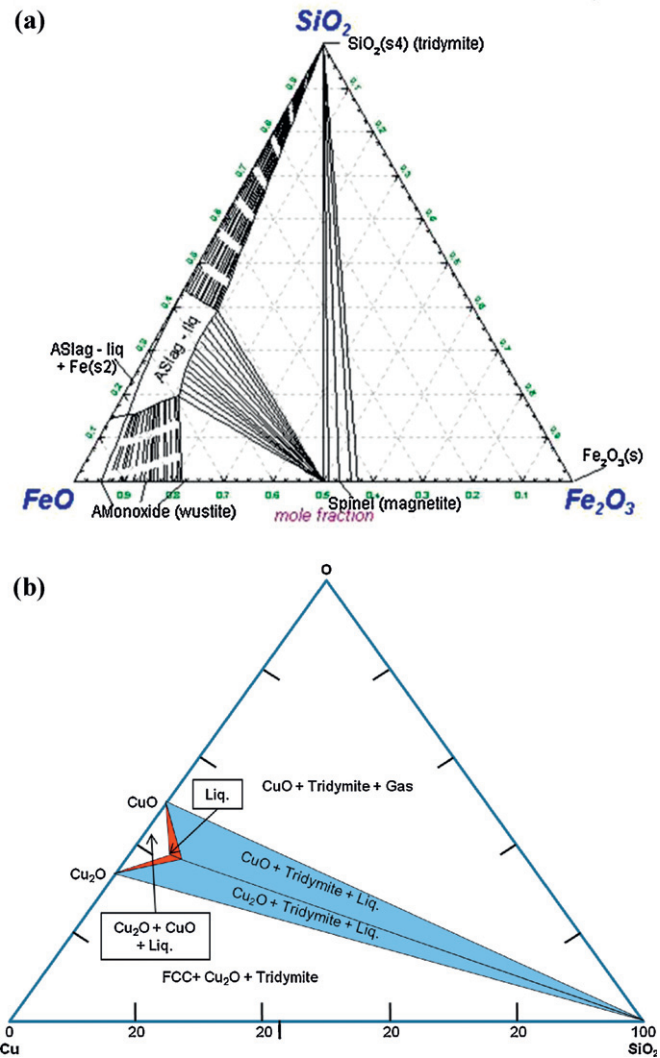


Fig. 10. Isothermal sections of (a) of FeO–Fe<sub>2</sub>O<sub>3</sub>–SiO<sub>2</sub> at 1300 °C and (b) Cu–O–SiO<sub>2</sub> phase diagram at 1100 °C.

Comparing to SiC, Si on the disc surface has relatively lower eutectic temperatures with metallic constituents in the debris, e.g. 802 °C for Si–Cu, though it is still high for Si–Fe (1212 °C).<sup>27</sup> This implies that Si and Cu could be jointed together through melting fusion at temperatures significantly lower than 1000 °C. Evidence for such fusion bonding is shown in Fig. 5. It should be pointed out that the existence of oxygen in some places, apart from Si and Cu, raises the fusion temperature above the eutectic temperature of Si–Cu, but fusion may still become possible as the temperature during braking could be well above the eutectic temperature unless the oxygen content is too high. Note, we did not see any direct bonding between steel debris and silicon on the interface in this study.

If there is no fusion bonding, ceramic constituents and metals can still be joined together on the basis of adhesion bonding, because a significant amount of metallic materials exist in the transferred materials. In material joining sector, this is also called brazing joining. To predict the adhesion joining, the following relationship is well established between melt and solid surface

(here ceramic constituents on the surface of disc) to predict the possibility of adhesion bonding:

$$\gamma_{SL} = \gamma_{SV} - \gamma_{LV} \cos \theta \quad (2)$$

Here  $\gamma_{SL}$ ,  $\gamma_{SV}$ ,  $\gamma_{LV}$  denote the liquid–vapour, solid–liquid and solid–vapour surface energy respectively, and  $\theta$  the contact angle between liquid and solid, i.e. the wetting angle. When  $\gamma_{SL} > \gamma_{SV}$ , the  $\theta$  is greater than  $90^\circ$ , no spreading occurs, i.e. the liquid drop tends to spheroidise. In contrast, when  $\gamma_{SL} < \gamma_{SV}$ , the  $\theta$  is smaller than  $90^\circ$ , the solid surface will be covered by a thin film of liquid, spreading along the surface of solid.

Studies have shown that for pure copper, the wetting angles are well above  $90^\circ$  on the surface of carbon and silicon carbide at temperature up to  $1000$ – $1100^\circ\text{C}$ .<sup>28</sup> This fact implies that pure copper existing in the debris can no longer be bonded with C and SiC on the composites surface, even if a high temperature reaches up to  $1000^\circ\text{C}$  on the friction surface of the current study. In the joining sector, however, much effort has been drawn to improve the wetting ability of copper by using active elements. Most of these are IVB elements such as Ti, Zr, Hf, and others such as Ni, Be, Cr, V, In and Co (a range of references on development of active filler metal are available from a review paper on advances in brazing of ceramics<sup>29</sup>). These active elements can reduce the wetting angle to less than  $90^\circ$ . In our study, EDX analysis either in SEM or TEM did not detect any of such active elements. Nevertheless, Cu + Si was detected on the interface over SiC when cross section TEM/EDX was applied on a friction surface after car testing. Literature shows that the wetting angles of Cu + Si are around  $30$ – $40^\circ$  at a temperature  $>1100^\circ\text{C}$ .<sup>24</sup> Therefore, even without the active elements, the studied transfer layer can be bonded on the surface of SiC, only when the temperature on the friction surface is high enough.

The wetting angle between Cu and Si is significantly smaller than  $90^\circ$ . For instance, it was shown that, at  $1100^\circ\text{C}$ , the wetting angle can quickly drop to  $6^\circ$  from initial  $45^\circ$ .<sup>30</sup> However, as the aforementioned temperature of fusion between Si and Cu is significant lower than  $1100^\circ\text{C}$ , we therefore believe fusion bonding likely superseded the adhesion bonding in Si regions.

Based on the above analysis, we could conclude that although the temperature on the friction surface might have reached around  $1000^\circ\text{C}$ , and a pressure up to a few hundreds MPa, it might not have been high enough to facilitate any possible bondings between the transfer layer and SiC + Si on the surface of the disc, apart from the fusion bonding between Cu and Si which has a significantly lower melting temperature than  $1000^\circ\text{C}$ . Note, no bonding was seen between Fe and Si in our study, and it should be another evidence to support that the temperature on the friction surface is lower than  $<1200^\circ\text{C}$  at least.

#### 4.3. Mechanical damage in the near surface of the composites

Cross section microstructure analysis has indicated that mechanical damage occurred in carbon and SiC, whilst it was

rarely seen in silicon regions. In carbon regions, interfaces between carbon fibre and pyrolytic carbon regions are purposely weakened to provide the composite with enough damage tolerance, i.e. crack propagation resistance, through the bifurcation of propagating cracks.<sup>31</sup> The weakness of the interface did provide preferred sites for harder debris to penetrate in, as seen in Section 3, and simultaneously for mechanical damage through microcracking. These microcracks could liaison together to generate large cracks on the surface, which leads to a dislodgment of carbon materials from the friction surface.

Detailed analysis of the friction surface has further reinforced the previous conclusion that surface damage did happen inside SiC regions through cracking at a small scale. This damage was likely due to the interaction of ductile deformation slips under a smearing condition, as shown in Fig. 8. Across each domain or grain, slipping was clearly developed, and these slips from difference adjacent domains interacted each other, which may lead to microcracking.

## 5. Summary

The cohesive structure was exposed by cross section TEM both inside the friction transfer layers and across their bonding interface on the surface of the carbon fibre reinforced ceramic composites after multi braking stop was applied by a pad containing an organic lining material. The transfer layer comprises metallic (mainly Fe alloys) debris consisting of refined grains with a size in sub-microns and fine grained regions where the nano-sized crystallites (mainly magnetite) either dispersed in an amorphous silicon or were packed together possibly through sintering at a temperature of  $\sim 1000^\circ\text{C}$  under an exceedingly high pressure. Inside the layer, silicic matters existed commonly in various formats from crystal to amorphous, and demonstrated clear benefits in developing the cohesion of the whole friction surface.

Analysis has supported a fact that a continuous friction transfer layer was successfully developed on the surface of contacted Si regions through a fusion bonding of Si and Cu, but no such a layer on that of SiC and C likely due to the temperature on the friction surface was not high enough for any fusion or brazing bindings under the current testing context.

Mechanical damage existed in both SiC and C<sub>f</sub>/C regions, but not in Si ones. Dense slips and stacking faults were developed in SiC crystallites near the friction surface, and their interactions led to microcracking. In C<sub>f</sub>/C regions, microcracks appeared along the interfaces between fibre and matrix, as well as abrasion-induced amorphisation on the contacted surface of carbon fibres. Cracking on the surface could reduce the sustainability of transfer layers in SiC and C regions.

## Acknowledgements

The authors would like to acknowledge the EPSRC and the Technology Strategy Board in UK for providing financial support for this research and Y.W.'s studentship.

## References

- Krenkel W, Heidenreich B, Renz R. C/C–SiC composites for advanced friction systems. *Adv Eng Mater* 2002;**4**:427–36.
- Paris JY, Vincent L, Denape J. High-speed tribological behavior of a carbon/silicon carbide composite. *Compos Sci Technol* 2001;**61**:417–23.
- Jang GH, Cho KH, Park SB, Lee WG, Hong US, Jang H. Tribological properties of C/C–SiC composites for brake discs. *Met Mater Int* 2010;**16**:61–6.
- Wang Y, Wu H. Friction surface evolution of carbon fibre reinforced carbon/silicon carbide (C<sub>f</sub>/C–SiC) composites. *J Eur Ceram Soc* 2010;**30**:3187–201.
- Xiao P, Li Z, Xiong X. Microstructure and tribological properties of 3D needle-punched C/C–SiC brake composites. *Solid State Sci* 2010;**12**:617–23.
- Xu Y, Zhang Y, Cheng L, Zhang L, Lou J, Zhang J. Preparation and friction behavior of carbon fiber reinforced silicon carbide matrix composites. *Ceram Int* 2007;**33**:439.
- Rhee SK, Jacko MG, Tsang PHS. The role of friction film in friction, wear and noise of automotive brakes. *Wear* 1991;**146**:89–97.
- Jacko MG, Tsang PHS, Rhee SK. Wear debris compaction and friction film formation of polymer composites. *Wear* 1991;**133**:23–8.
- Eriksson M, Jacobson S. Tribological surfaces on organic brake pads. *Tribol Int* 2004;**33**:817–27.
- Österle W, Urban I. Third body formation on brake pads and rotors. *Tribol Int* 2006;**39**:401–8.
- Österle W, Dörfel I, Prietzel C, Rooch H, Cristol-Bulthé A-L, Degallaix G, et al. Comprehensive microscopic study of third body formation at the interface between a brake pad and brake disc during the final stage of a pin-on-disc test. *Wear* 2009;**267**, 781–188.
- Hinrichs R, Vasconcellos MAZ, Österle W, Prietzel C. A TEM snapshot of magnetite formation in brakes: the role of the disc's cast iron graphite lamellae in third body formation. *Wear* 2011;**270**:365–70.
- Österle W, Urban I. Friction layers and friction films on PMC brake pads. *Wear* 2004;**257**:215–26.
- Österle W, Kloß H, Urban I, Dmitriev AI. Towards a better understanding of brake friction materials. *Wear* 2007;**263**:1189–201.
- Leatherbarrow A, Wu H. Understanding the development of the microstructure inside C<sub>f</sub>/C–SiC composites manufactured by liquid silicon infiltration. In: *Proc. 7th int. conf. high temp. cer. matrix comp. (HT-CMC 7)*. 2010. p. 308–13.
- Krenkel W, Berndt F. C/C–SiC composites for space applications and advanced friction systems. *Mater Sci Eng A* 2005;**412**:177–81.
- Zou L, Huang B, Huang Y, Huang Q, Wang C. An investigation of heterogeneity of the degree of graphitization in carbon–carbon composites. *Mater Chem Phys* 2003;**82**:654–62.
- Murdie N, Ju CP, Don J, Fortunato FA. Microstructure of worn pitch/resin/CVI C–C composites. *Carbon* 1991;**29**:335–42.
- Chen JD, Ju CP. Effect of sliding speed on the tribological behavior of a PAN–pitch carbon–carbon composite. *Mater Chem Phys* 1995;**39**:174–9.
- Derby B. The dependence of grain size on stress during dynamic recrystallization. *Acta Metall Mater* 1991;**39**:955–62.
- Takeuchi S, Argon AS. Steady-state creep of single-phase crystalline matter at high temperature. *J Mater Sci* 1976;**11**:1542–66.
- Meco H, Napolitano RE. Liquidus and solidus boundaries in the vicinity of order–disorder transitions in the Fe–Si system. *Scr Mater* 2005;**52**:221–6.
- Clarke DR, Kroll MC, Kirchner PD, Cook RF. Amorphization and conductivity of silicon and germanium by indentation. *Phys Rev Lett* 1988;**60**:2156–9.
- Liu GW, Muolo ML, Valenza F, Passerone A. Survey on wetting of SiC of molten metals. *Ceram Int* 2010;**36**:1177–88.
- Blomberg A, Hogmark S, Lu J. An electron microscopy study of worn ceramic surfaces. *Tribol Int* 1993;**26**:369–81.
- Rannikke H. A thermodynamic assessment of the Cu–O–CaO–SiO<sub>2</sub>. *Syst Acta Polytech Acta Polytech Scand Chem Technol Ser* 1995;**229**.
- Massalski TB. *Binary Alloy Phase Diagrams*. 2nd ed. Metals Park, Ohio: ASM Int.; 1990.
- Gnesin GG, Naidich YuV. Contact reaction of SiC with fused Cu. *Poroshka Met* 1969;**74**:57–63.
- Akselsen OM. Review advances in brazing of ceramics. *J Mater Sci* 1992;**27**:1989–2000.
- Protsenko P, Kozlova O, Voytovych R, Eustathopoulos N. Dissolution wetting of Si by molten Cu. *J Mater Sci* 2008;**43**:5669–71.
- Kim KC, Yoon KJ, Pickering R, Sherwood PJ. Fracture toughness of 2-D carbon fibre reinforced carbon composites. *J Mater Sci* 1985;**20**:3967–75.